Fabrication and Characterization of ZnO:CuO electronic composites for their application in sensing processes.

D. J. Ramos-Ramos, B. Sotillo, A. Urbieta, P. Fernández‡

Abstract— **Sensing behaviour of samples belonging to the system ZnO:CuO has been investigated. Samples with different proportions of ZnO and CuO have been sintered and exposed to a reducing agent as ethanol (C_2H_5OH). All the samples have been characterized not only from the point of view of the sensing properties but also regarding morphology, composition, crystallinity and luminescent properties in order to correlate these properties to the sensing behaviour. Sensitivity, response times, recovery and stability have been measured under exposure to ethanol vapour in concentrations 800, 4700 and 16000 ppm. Sensing cycles have been performed at three different temperatures: 25, 50 and 100°C.**

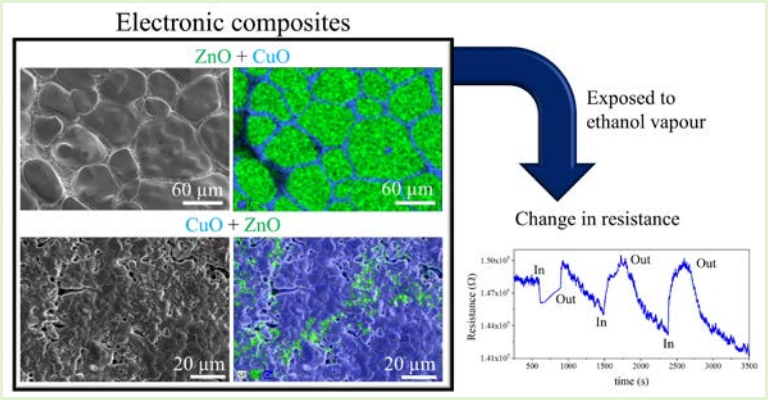

***Index Terms*— P-n junctions, Semiconductor devices, Gas detectors, Semiconductor detectors, Sensor phenomena and characterization.**

I. Introduction

The development of more reliable sensors becomes ever more important since the sources of toxic or pollutant substances are increasing every day. The need of more sensitive devices affects to natural and industrial environments, but also is a very important issue in public health. The detection of low concentrations of hazardous gases is extremely important to reduce to the damage to environment and of course to the people. A large variety of industrial emissions could be substantially reduced with more efficient sensing devices. An adequate application of sensing technology could also help to optimize many industrial processes in terms of both energy and emissions [1]. Many different types of sensors may be used to the detection of gases, in each case exploiting different properties of the materials, a colour change, fluorescent emission or reflectance change in the case of the optical sensors [2], or changes in any electrical property in the electrical sensors. Not only the resistivity is susceptible to be used for the transducing function, changes in the band structure in field effect transistors (FET) [3] or metal-insulator- semiconductors (MIS) have been also used to monitor the presence of gases and nitro compounds [4].

Among the different type of sensors, those made from ceramic oxides are receiving much attention due not only to their good properties but also to their chemical stability and fabrication easiness. Compared to other type of sensors, semiconductor metal oxide (SMO) gas sensors show excellent sensitivity and response time ([5, 6, 7]). They are very stable and durable, and their accuracy is good. Their maintenance, cost and portability are also excellent. The only disadvantageous point of these sensors when compared to other like those based on infrared absorption is selectivity. However, considering all the properties jointly, SMO are undoubtedly the best option [8].

In ceramic oxide semiconductors several interaction paths with the ambient are found: bulk grains, intergranular junctions and interfaces between the oxide and the electrode. In all cases, the interaction involves the transfer of electrons and hence a change in resistivity, however the mechanisms behind each path bring about some differences on the sensing behaviour. In the case of bulk grain sensing, stoichiometry of the oxide may change due to changes in the ambient gas, the separation from ideal stoichiometry will bring either holes or electrons in excess and hence a change in the conductivity that can be related to the oxygen partial pressure, P_{O2}:

‡Department of Materials Physics, Faculty of Physics, Complutense University of Madrid, Madrid, Spain (e-mail: anaur@fis.ucm.es).

$$\sigma = \sigma_0 \exp\left(-\frac{E_a}{kT}\right) P_{O_2}^{\pm\frac{1}{n}}$$

where n is related to the type a bulk defect dominating the equilibrium, E_a is the activation energy for conduction, σ_0 is a constant and k is the equilibrium constant. Although this model is usually applied at higher temperature ranges, we will assume that in our case it is valid, at least for a phenomenological approach.

Since the main defect in metal oxides are usually oxygen related, mostly doubly charged oxygen vacancies, the defect equilibrium equation could be written as

$$O^x = V_{\ddot{O}} + \frac{1}{2}O_2 + 2e^-$$

and the equilibrium constant

$$k = [V_{\ddot{O}}][e]^2[P_{O_2}]^{1/2}$$

For charge neutrality requirements $[V_{\ddot{O}}]=2[e^-]$, hence the electron concentration becomes proportional to $P_{O_2}^{-1/6}$, and the value of n would then be -6 for this example [9].

When the interaction path is the surface layer between grains, the interaction with the different species in the ambient gas may cause important modifications on the defect structure, and hence the defect electronic levels, of the surface layer. The depletion or accumulation layer will dominate over the bulk processes, giving rise to a surface-controlled sensing mechanism [10].

Finally, in metal/oxide junction controlled sensors, the interaction, and subsequent adsorption, of ambient gas species with the interface may cause changes either in the resistance (in Schottky barrier diodes) or in the flat band voltage (in MOS/MOSFET devices). An excellent review of the different sensing mechanism in ceramics oxides are the works of Park and Akbar [1] and Dey [9].

In this work we focus on the system ZnO:CuO. Transition metal semiconductor oxides have been used on numerous occasions for sensing harmful gases [11, 12, 13]. Among these semiconductors ZnO is a semiconductor that normally behaves as an n type, and CuO is a semiconductor that generally has a p-type behaviour. This combination opens a good opportunity to investigate the evolution of the sensing properties on moving from n- to p-type conductivity and the sensing properties of p-n junctions of different materials [14, 15, 16]. On the other hand, the large segregation effects observed in this system [17, 18] gives us the opportunity to investigate the enhancement of sensing behaviour of the composites [19, 20, 21]. Finally, n-p junctions made with ZnO and CuO nanowires have shown to be a good option to control the selectivity of the sensor [10].

II. CHARACTERIZATION

The morphological characterization of the samples has been carried out using scanning electron microscopy (SEM) techniques, in a LEICA Stereoscan 440 microscope. X-ray dispersion spectroscopy (EDX) has been used to obtain the chemical composition. EDX has been performed with a Bruker AXS Quantax system attached to the LEICA Stereoscan 440 microscope. Micro-Raman spectroscopy has been carried out in a Horiba Jobin Yvon LabRAM HR800 Confocal microscope with a focused He-Ne red laser as an excitation source (λ = 632.8 nm). Luminescent properties have been characterized by means of photoluminescence (PL). PL was performed in the confocal microscope, using a He-Cd laser as excitation source (λ = 325 nm). Finally, once the samples have been characterized, Au has been evaporated to create the electrodes to measure the variation in resistance after gas exposure. The resistivity has been measured with a two-points configuration using a KEITHLEY 2410 multimeter. Temperature has been controlled using an Oxford Intelligent Temperature Controller (ITC4). The set up used for sensing measurements is shown in figure 1.

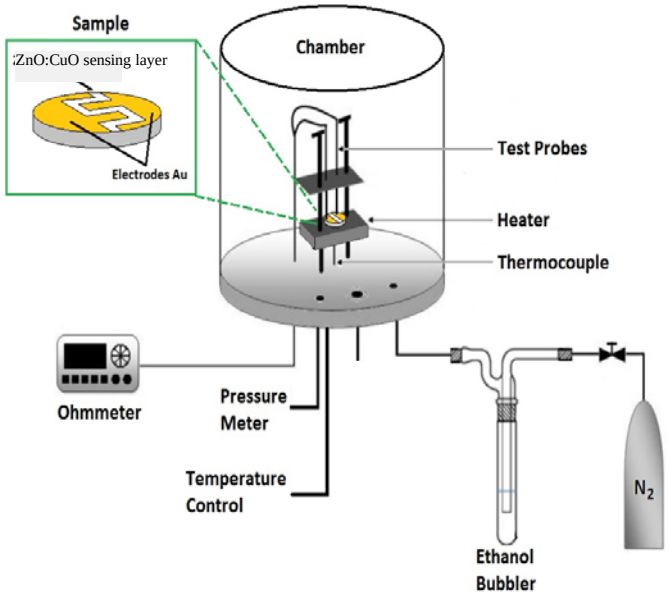

Fig. 1. Setup for the sensing experiments.

III. RESULTS AND DISCUSSION

According to de SEM and EDX observations, the samples can be classified into five series, based on the composition and morphology. i) CuO content between 0 to 1 weight %. In this region no segregation has been observed. ii) CuO content between 1 to 30 weight % where a clear phase segregation is observed. Regions iii and iv with CuO content between 50 to 70 weight % and 70 to 1 weight % respectively, showing segregation and significant changes in grain morphology. And finally, the region corresponding to CuO content between 99 to 100 weight % which shows no segregation, as in the case of region i, but where the grain structure is quite different to that

found in ZnO rich samples. As a general observation, regardless the segregation effects, the grain size decreases as the CuO content increases.

Focusing on each group of samples, great differences have been found in the phases' distribution. Figure 2 shows the grain structure (part a) and Zn and Cu distribution (parts b and c) for samples where CuO content varies from 0 to 1 wt%. As it is clearly observed, a well-defined grain structure with sizes of tens of microns is formed, however, both Zn and Cu distribution are homogeneous along the sample indicating that no segregation is present for these low CuO contents.

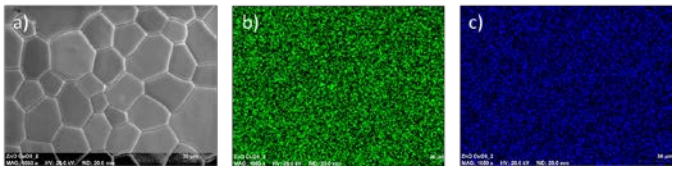

Fig. 2. Scanning microscopy images of the samples with 1 wt% CuO content. a) Secondary electron image; b) EDX map for Zn; c) EDX map for Cu.

As the CuO content increases in the initial mixture (1-30 wt% CuO), although the grain structure appears similar to the former samples (figure 3a), a clear differentiation of phases can be seen. As the EDX maps show (part b and c), the grains are mainly composed of Zn and the intergranular space is Cu, suggesting that a segregation of CuO towards the grain boundaries has been occurred.

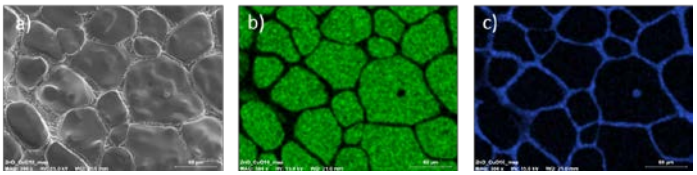

Fig. 3. Scanning microscopy images of the samples with 10 wt% CuO content. a) Secondary electron image; b) EDX map for Zn; c) EDX map for Cu.

A further increase in CuO leads to a change in grain morphologies. Figure 4 shows SE images (part a), Zn (part b) and Cu (part c) maps of a sample with 50 wt% of CuO. As for lower CuO contents, CuO and ZnO grains appear clearly segregated, however in this case, well faceted microcrystals of CuO appear preferentially on the grain boundaries.

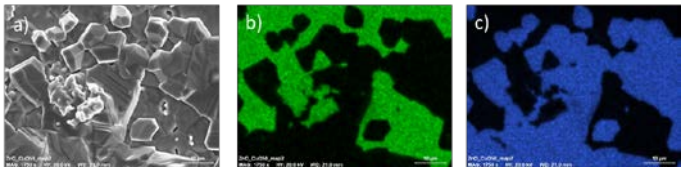

Fig. 4. Scanning microscopy images of the samples with 50 wt% CuO content. a) Secondary electron image; b) EDX map for Zn; c) EDX map for Cu.

For samples with the highest CuO content (above 90 wt%) the predominant morphology are uneven small grains of ZnO and CuO alternating (Figure 5). As we increase the wt% of CuO, the number of ZnO grains that decorate the CuO decreases until the ZnO is incorporated into the CuO indistinguishably. For the sample of 99 wt% of CuO (Figure 6), a granular morphology is obtained in which the EDX maps show no phase segregation to the boundaries. Some ZnO particles can be observed randomly distributed, but Zn seems to be homogeneously distributed through both grains and boundaries.

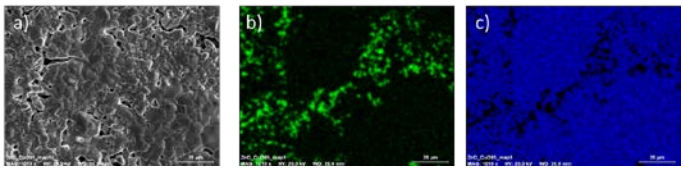

Fig. 5. Scanning microscopy images of the samples with 95 wt% CuO content. a) Secondary electron image; b) EDX map for Zn; c) EDX map for Cu.

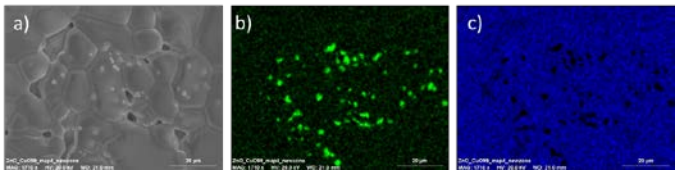

Fig. 6. Scanning microscopy images of the samples with 99 wt% CuO content. a) Secondary electron image; b) EDX map for Zn; c) EDX map for Cu.

The presence of the different phases mentioned above can be further assessed by micro-Raman spectroscopy. Table I summarizes the position of main Raman modes that can be measured in both ZnO and CuO. These Raman peaks are observed in the different regions of the samples. To illustrate the Raman characteristics, samples from series i, ii, iv and v have been selected (Fig. 7).

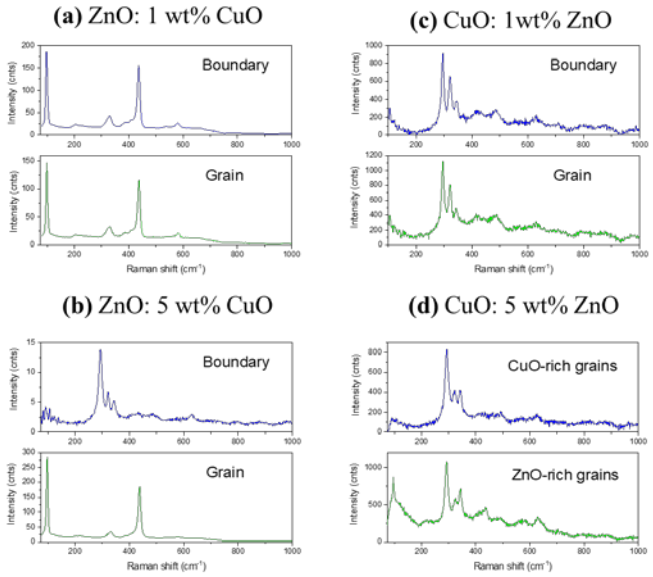

Fig. 7. Micro-Raman spectra (λexc = 632.8 nm) recorded on different regions of various samples: (a) ZnO:1 wt% CuO (sample from series i). (b) ZnO:5 wt% CuO (sample from series ii). (c) CuO:1 wt% ZnO (sample from series v). (d) CuO: 5 wt% ZnO (sample from series iv).

TABLE I
ZNO (WURTZITE STRUCTURE); CUO (MONOCLINIC STRUCTURE) AND Cu_4O_3 (TETRAGONAL STRUCTURE) RAMAN MODES OBSERVED IN THE SAMPLES, ALONG WITH THE ASCRIPTION OF EACH MODE.

Observed peaks ZnO	Mode Ref. [22, 23, 24]	Observed peaks CuO	Mode Ref. [25, 26]	Observed peaks Cu_4O_3	Mode Ref. [25]
98 cm^{-1}	E_2^{low}				
		295 cm^{-1}	A_g		
				321 cm^{-1}	E_g
329 cm^{-1}	E_2^{high}-E_2^{low}				
		345 cm^{-1}	B_g (1)		
385 cm^{-1}	A_1 (TO)				
409 cm^{-1}	E_1(TO)				
436 cm^{-1}	E_2^{high}				
582 cm^{-1}	E_1 (LO)				
		631 cm^{-1}	B_g (2)		

As we have described before, samples of ZnO with a CuO content below 1 wt% show no segregation of elements (Figure 2). In these samples, no difference is observed between the Raman spectrum recorded on the grain and the spectrum recorded on the boundaries (Figure 7a). All the modes observed in Figure 7a can be related to the ZnO wurtzite structure (Table I), being the most intense and sharp those corresponding to the non-polar optical modes E_2^{low} and E_2^{high}. The narrowness of both peaks is an indication of the good crystal quality of the ZnO grains despite the Cu incorporation.

When the CuO content increases above 1 wt%, Cu segregation is observed towards the grain boundaries (Figure 3). In the Raman spectra (Figure 7b) the difference between the spectra recorded on the grains and on the boundaries is clear. Grains present peaks related to ZnO, whereas boundaries only have peaks associated to CuO and Cu_4O_3 compounds (Table I).

On the other side of the series, where the dominant compound in the samples is CuO, similar differences can be observed depending on the occurrence or not of segregation. For the samples with a composition of CuO with a wt% of ZnO below 1, no segregation is detected in EDX measurements (Figure 5) and the Raman spectra recorded on both grains and boundaries are the same (Figure 7c). The peaks detected can be ascribed to the CuO monoclinic structure and to the Cu_4O_3 tetragonal structure (check Table I). This indicates that part of the starting CuO material is transformed into Cu_4O_3 during the thermal treatment.

For the samples of CuO with a wt% of ZnO above 1, segregation of Zn has been observed, but not towards the grain boundaries but to form small ZnO grains (Figure 4). The Raman spectra recorded on the CuO-rich grains again show peaks related to the CuO and Cu_4O_3 phases (Figure 7d). On the other hand, the Raman spectra of the ZnO-rich grains (Figure 7d) have the two most intense Raman modes observed in ZnO (non-polar optical modes E_2^{low} and E_2^{high}) along with the CuO and Cu_4O_3 related modes. As ZnO grain have small size in this samples in comparison with the laser spot of the confocal microscope, it cannot be discarded that the CuO and Cu_4O_3 signals come from the surrounding CuO-rich grains.

Photoluminescence spectra have been recorded from all the samples (Fig. 8), the spectra of the samples containing 1 wt% and 30 wt% of CuO are shown. Two different spectral regions are distinguished. i) A band centred at 382 nm (UV) corresponding to the band edge emission of ZnO. For the rest of samples not shown, the PL spectra is similar as Fig. 8. It can also be observed in this area that a modulation is superimposed to the main band, the separation of the modulated peaks is approximately 8 nm, which is due to a resonant Raman emission of LO phonons of ZnO [25]. ii) A second region with high emission intensity, is centred at 525 nm and is present in all the samples. This band could be attributed to deep level centres [27]. As the ZnO concentration decreases we see how the intensity of this band decreases. This is caused by the incorporation of Cu ions in the lattice of ZnO. Thus, we can assume that an incorporation of Cu ions in ZnO host lattice exist even having a low solubility limit of Cu ions in ZnO [28].

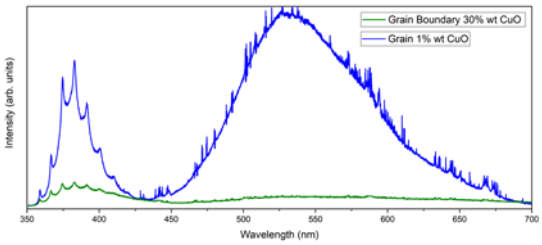

Fig. 8. Photoluminescence spectra (λ_{exc} = 325 nm) recorded at a grain (1 wt% CuO) and a boundary (30 wt% CuO).

To analyse the sensing properties, we have exposed the samples to a reducing agent: ethanol, and the changes in resistance have been measured. As we have mentioned in the introduction, ZnO has electrons as the majority carriers, so it is type n, while CuO has holes as main carriers, so it is type p. Thus, we are faced with ceramic samples in which, depending on the morphology, we have p-n, p-p or n-n junctions what will strongly affect the sensing behaviour, that have been observed to be extremely complex.

First, we will give an overview of the sensitivity and response time as a function of the composition, for the whole set of samples.

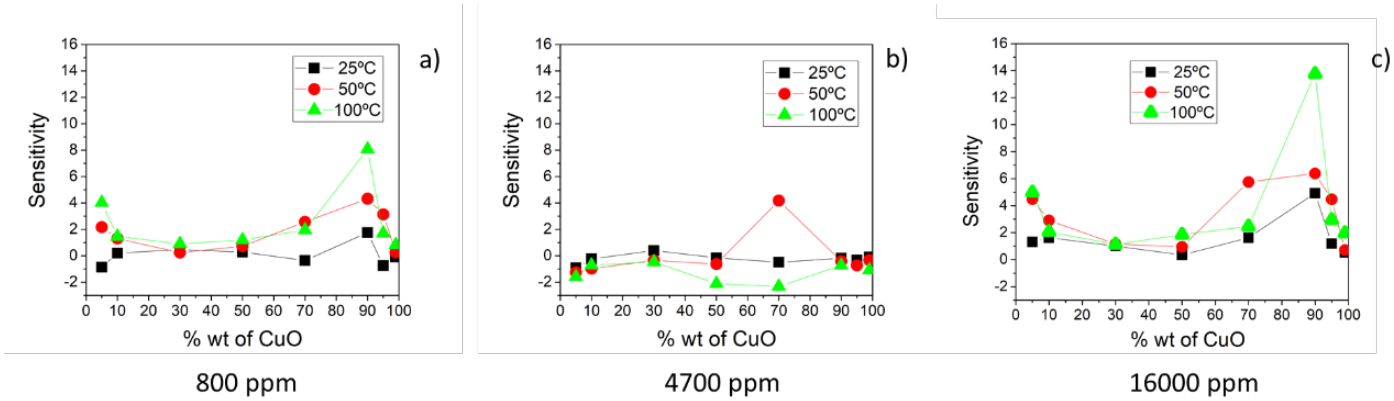

Fig. 9. Evolution of sensitivity as a function of composition, temperature (different colours in each graph) and gas concentration: a) 800 ppm; b) 4700 ppm and c) 16000 ppm. The lines linking experimental points are shown as an eye-guide.

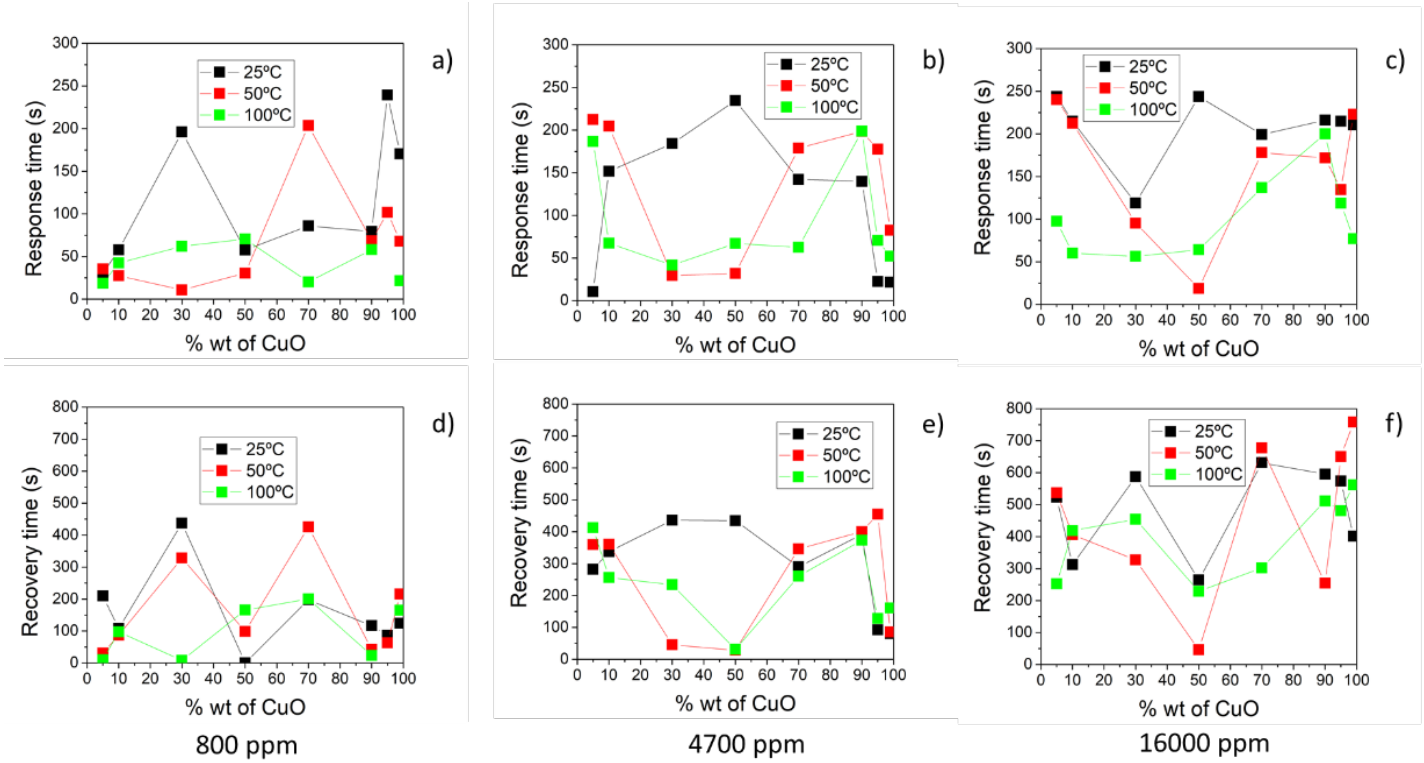

Fig. 10. Evolution of response (a, b, c) and recovery (d, e, f) times as a function of composition, temperature (different colours in each graph) and gas concentration: a, d) 800 ppm; b, e) 4700 ppm and c, f) 16000 ppm. The lines linking experimental points are shown as an eye-guide.

The sensitivity has been calculated with the following equation:

$$S = 100\frac{R - R_0}{R_0}$$

Where R_0 is the base resistance, and R is the maximum change of resistance in the exposition to the ethanol. While the samples are being exposed to the ethanol, a negative sensitivity means a decrease response in the resistance and a positive sensitivity implies a rise in the resistance during the exposition.

In all cases the maximum sensitivity is observed for the Cu rich samples, however some differences are found. For low and higher gas concentration (800 ppm and 16000 ppm, figure 9a and 9c, respectively) the maximum sensitivity is found at 100°C while for medium gas concentration (4700 ppm, figure 9b) the maximum sensitivity is observed at 50°C. As we said before, it can be observed in this figure that sensitivity changes from negative to positive values, indicating that the exposure to gas has provoked a decrease or an increase in resistivity, respectively. For n-type semiconductor exposed to a reducing atmosphere a decrease in the resistivity is expected, while the opposite should be observed for p-type materials, then either the different phases (Cu-rich or Zn-rich) dominate in the different regimes or, as it will be discussed later, a transition p-n sensing is produced. Similar differences have observed in a previous work in which different precursors were used to produce the Cu doped ZnO ceramics [17].

Figure 10 shows the response and recovery times, defined as the time that must elapse for a 90% change in resistance to occur and before the resistance returns to 90% of the state prior to exposure to the gas respectively. Response and recovery times show a quite erratic behaviour, most likely since we have different sensing channels as we will see later. Nevertheless, as seen from figure 10, the intermediate composition range seems to be a good compromise for temperatures of 50° and 100°C where both parameters have very low values.

For a deeper analysis we have selected two samples, one at each extreme of the series, in particular ZnO: 5 wt% CuO and CuO: 5 wt% ZnO. In the samples under study we have basically three different elements that can contribute to the changes in resistance. These three elements are present in different proportions depending on the microstructure. As have been discussed, first we have segregated grains of both ZnO (n-type) and CuO (p-type), consequently we can find three different types of grain boundaries: n-n, p-p or n-p. The dominance on any of these junctions will affect the transduction function considerably [12], as shown in the scheme of figure 11.

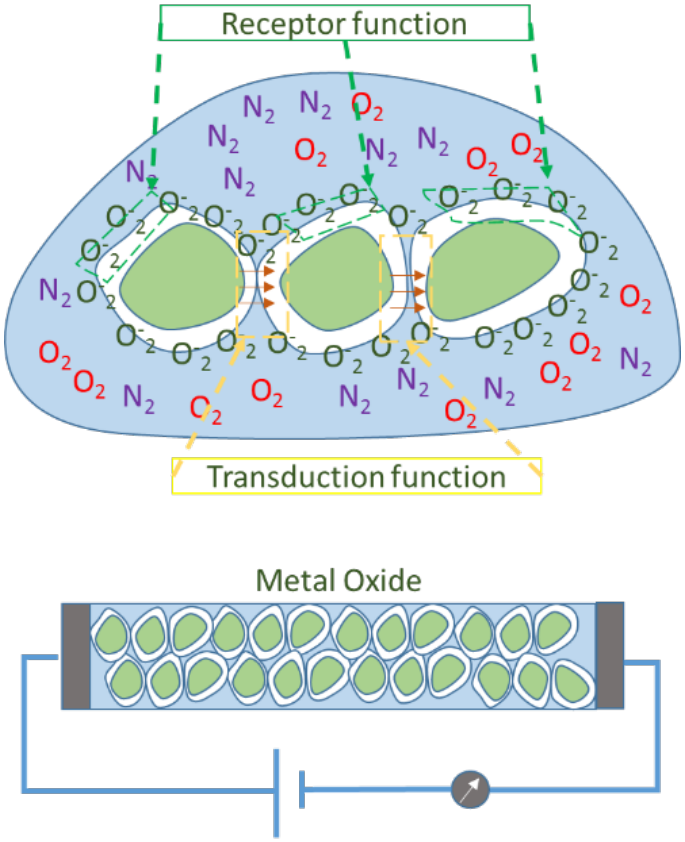

Fig. 11. Scheme of the different elements involved in the sensing mechanism: Receptor function (green) and Transduction function (yellow). The lower part of the scheme shows the equivalent circuit.

In the case of n-n junctions a depletion layer is formed, i.e., the electrons (majority carriers) must overcome the barrier fig 12a); in the case of p-p junction an accumulation layer is formed, i.e., the majority carriers are now holes and they do not find any obstacle on passing through the junction (fig 12b). When ZnO and CuO grains are adjacent to each other, a p-n junction forms, i.e., holes may travel through the junction without problem, but electrons must overcome the barrier associated to the band offset (fig.12c). The sensing behaviour of electric composites have been already described for several oxide systems by Korotcenkov [8, 20] and in particular for CuO-ZnO arrays by Park et al [10] and SnO_2 nanorods modified with ZnO by Huang et al [29].

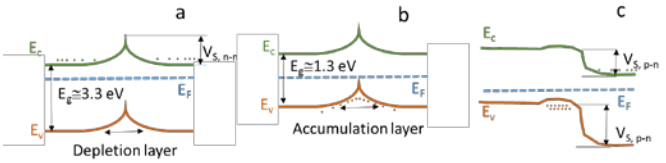

Fig. 12. Flat band scheme showing the accumulation and depletion regions formed at the different kind of junctions. a) n-n; b) p-p and c) p-n.

According to the work of Jun et al. [30] the situation we have at both extremes of the series could be represented by the equivalent circuits shown in figure 13. Type I for ZnO rich samples, and type II for CuO rich samples.

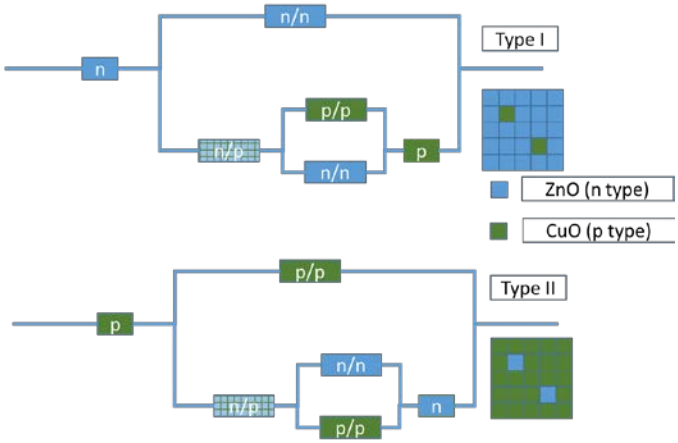

Fig. 13. Equivalent circuits for type I (ZnO rich) and type II (CuO rich) samples.

The type I sample (ZnO. 5 wt% CuO) shows a change from n- to p- sensing behaviour at all temperatures. At 25°C an initial rapid decrease of resistance is observed, then it increases, steadily until the gas flow is closed. The maximum values of resistance reached in each cycle are progressively lower, indicating that recovery is very low, as could be expected for this low temperature. Only at the highest gas exposure level (>16000 ppm) an increase in the resistance is observed after the initial strong decrease. At the highest temperature (100°C), an initial decrease of the resistance upon exposure to low concentration of ethanol (800 ppm) (figure 14) is observed, then at higher ethanol concentration the opposite response is observed, resistivity clearly increases thus indicating a transition to p-type behaviour. At the intermediate temperature, 50°C, a mixed behaviour is observed. At low gas concentrations, it is similar to the behaviour at high temperature. At 4700 ppm we already have a p-type behaviour, but as observed for 25°C, the resistance increases

steadily without reaching a stable value. Above 16000 ppm, still no steady value is reached, but the increase in the resistance upon gas exposure is clearly observed. In the work of Huang et al [29] a similar behaviour is attributed to the introduction of shallow donors that would contribute with electrons to the p regions, in our case the grain boundaries where the CuO is segregated, causing a decrease in the majority carriers and hence an increase in resistivity. On the other hand, at the low temperatures used in this work adsorption-desorption kinetics might play a crucial role, most likely responsible for the difficulty to reach the steady resistance value. The change in the response with temperature could also be related to the species that are already adsorbed on the surface: oxygen, water vapour [1, 31]. As the temperature increases, they desorb more and allow more ethanol molecules to interact with the semiconductor surface. At lower temperatures, ethanol molecules can interact with both the adsorbed molecules and the semiconductor surface, producing a less common behaviour.

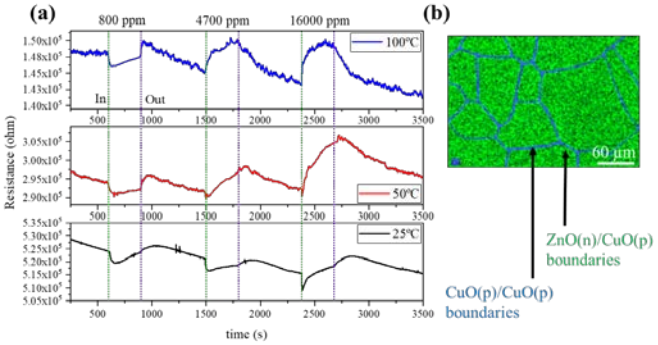

Fig. 14. (a) Resistance measurements performed on ZnO: 5 wt% CuO sample. The sample has been exposed to different concentrations of ethanol (800, 4700 and 16000 ppm) at three different temperatures (25, 50 and 100°C). (b) EDX mapping of the ZnO: 5 wt% CuO tested sample, showing the ZnO grains (in green); CuO-CuO boundaries (in blue) and ZnO-CuO boundaries (between green and blue regions).

As shown in figure 15, in the type II samples, the sensing behaviour at 100°C is clearly p-type as corresponds to CuO. At low temperatures however, we still have a change in the behaviour for the lower gas concentrations, which could be related to adsorption-desorption kinetics. At 50°C, only at very low gas concentrations a slight decrease in the resistivity is observed. The interaction of the gas at this stage would have place with the ZnO (n)-CuO (p) junction regions. As the gas concentration increases more electrons would be injected to the more abundant CuO-CuO interfaces and hence majority carriers could be partially compensated and the resistivity would increase. At 25°C the same tendency is observed but the threshold concentration for the onset of p-type behaviour is higher. On the other hand, the response seems to be more stable at higher temperatures, where a rapid increase of resistance is observed to reach an almost constant value and then a rapid decrease upon gas flow switch off. At lower temperatures both changes, increase and decrease, are quite slow, in agreement with the response and recovery times observed.

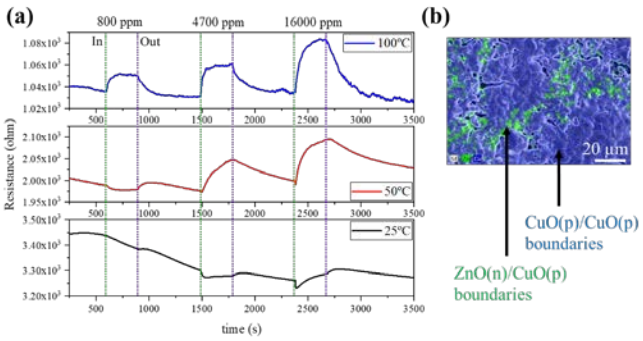

Fig. 15. (a) Resistance measurements performed on CuO: 5 wt% ZnO sample. The sample has been exposed to different concentrations of ethanol (800, 4700 and 16000 ppm) at three different temperatures (25, 50 and 100°C). (b) EDX mapping of the CuO: 5 wt% ZnO tested sample, showing the ZnO grains (in green) and the CuO grains (in blue). The boundaries mainly present in this sample are CuO-CuO and CuO-ZnO boundaries, as indicated in the image.

IV. CONCLUSIONS

The system ZnO:CuO has been investigated over the whole composition range. The morphology of the samples varies dramatically with the composition. In general, strong segregation of Zn-rich (n-type) and Cu-rich (p-type) phases and changes in the grain sizes are observed. The formation of electronic composites associated to the different kind of junctions (n-n; p-p and n-p) provokes the change between p-type and n-type sensing behaviour. Sensing cycles performed at low temperatures (25, 50 and 100°C) suggest that the system ZnO:CuO is suit for the gas detection and opens the possibility to fabricate a multiresponse device combining p- and n- type regions.

ACKNOWLEDGMENT

The authors are grateful to the Complutense University of Madrid and Banco Santander for support via the project UCM Santander 2019 (PR87/19-22613) and the Spanish Ministry of Science, Innovation and Universities for support via the project MINECO/FEDER-MAT2015-65274-R.B.Sotillo acknowledges financial support from Comunidad de Madrid (Ayudas del Programa de Atracción de Talento, 2017-T2/IND-5465).

REFERENCES

[1] C. O. Park and S. A. Akbar, “Ceramics for chemical sensing,” J. Mat. Sci. **38** (2003), 4611-4637.

[2] G. Lim, U. P. DeSilva, N. R. Quick, and A. Kar, "Laser optical gas sensor by photoexcitation effect on refractive index," Appl. Opt. **49**, 1563-1573 (2010).

[3] B. M. Lowe, et al., ”Field-effect sensors–from pH sensing to biosensing: sensitivity enhancement using streptavidin–biotin as a model system,” Analyst, 2017, **142**, 4173.

[4] A.V. Litvinov, et al., "The detection of nitro compounds by using MIS-sensor," 2019 IOP Conf. Ser.: Mater. Sci. Eng. **498,** 012020.

[5] S. S. Rathnakumar, et al., "Stalling behaviour of chloride ions: A non-enzymatic electrochemical detection of α-Endosulfan using CuO interface," Sensors & Actuators B: Chemical, **293**, (2019), 100-106.

[6] K. Kaviyarasu, et al., "ZnO doped single wall carbon nanotube as an active medium for gas sensor and solar absorber," Journal of Materials Science: Materials in Electronics, **30**, (2019), 147-158.

[7] F. Fang, et al., "UV and humidity sensing properties of ZnO nanorods prepared by the arc discharge method," Nanotechnology, **20**, 24, (2009).

[8] G. Korotcenkov, "Metal oxides for solid-state gas sensors: What determines our choice?", Mat. Sc. And Eng. B **25,** (2007) 1-23.

[9] A. Dey, "Semiconductor metal oxide gas sensors: a review," Mat. Sci and Eng. B **229,** (2018) 206-217.

[10] W. J. Park., et al., "Self-Assembled and Highly Selective Sensors Based on Air-Bridge-Structured Nanowire Junction Arrays," ACS Appl. Mater. Interfaces **5**, (2013) 6802.

[11] N. Yamazoe, "Toward innovations of gas sensor technology," Sens. Actuators B, **108**, (2005), 2-14.

[12] I. D. Kim, et al., "Advances and new directions in gas-sensing devices," Acta Mater, **61**, (2013) 974-1000.

[13] P. Shankar, J. B. B. Rayappan, "Gas sensing mechanism of metal oxides: the role of ambient atmosphere, type of semiconductor and gases – A review", Sci. Lett. J. **4**, (2015) 126.

[14] M. Hümber, et al., "Influence of humidity on CO sensing with p-type CuO thick film gas sensors," Sens. Actuators B, **153**, (2011) 347-353.

[15] H. J. Kim, J. H. Lee, "Highly sensitive and selective gas sensors using p-type oxide semiconductors: Overview," Sens. Actuators B, **192**, (2014) 607-627.

[16] S. Aygün, D. Cann, "Hydrogen sensitivity of doped CuO/ZnO heterocontact sensors," Sensors and Actuators B **106**, (2005) 837–842.

[17] S. Señorís, B. Sotillo, A. Urbieta and P. Fernández, "Optical spectroscopy characterization of Cu doped ZnO nano- and microstructures grown by vapour-solid method," Journal of Alloys and Compounds, **687**, (2016) 161.

[18] A. Ramos, A. Urbieta, G. Escalante, P. Hidalgo, J.P. Espinós and P. Fernández, "Study of the influence of the precursors on the sensing properties of ZnO:Cu system," Ceramics International, **46**, (2020) 8358-8367 (doi.org/10.1016/j.ceramint.2019.12.068).

[19] D. H. Yoon, J. H. Yu, G. M. Choi, "CO gas sensing properties of ZnO–CuO composite," Sensors and Actuators B: Chemical **46**, (1998) 15-23.

[20] G. Uozumi, M. Miyayama, H. Yanagida, "Fabrication of a CuO-infiltrated ZnO composite and its gas sensing properties," Journal of Materials Science **32**, (1997) 2991-2996.

[21] G. Korotcenkov and B.K. Cho, "Metal oxide composites in conductometric gas sensors: Achievements and challenges," Sensors and Actuators B **244**, (2017) 182–210.

[22] R. Cuscó, E. Alarcón-Lladó, J. Ibanez, L. Artús, J. Jiménez, B. Wang & M. J. Callahan, „Temperature dependence of Raman scattering in ZnO," Physical Review B **75** (16), (2007) 165202.

[23] A. H. N. Melo, M. A. Macêdo, "Permanent data storage in ZnO thin films by filamentary resistive Switching," PLOS ONE **11**, (2016) 12.

[24] A. Calzolari & M. B. Nardelli, "Dielectric properties and Raman spectra of ZnO from a first principles finite-differences/finite-fields approach," Sci. Rep. **3** (1), (2013) 2999.

[25] L. Debbichi, et al., "Vibrational properties of CuO and Cu4O3 from First-Principles calculations, and Raman and infrared Spectroscopy," J. Phys. Chem. C **116**, (2012) 10232-10237.

[26] T. H. Tran & V. T. Nguyen, "Copper oxide nanomaterials prepared by solution methods, some properties, and potential applications: a brief Review," International Scholary Research Notices **2014**, (2014), 1-14.

[27] J. Kennedy, et al., "Investigation of structural and photoluminescence properties of gas and metal ions doped zinc oxide single crystals," Journal of Alloys and Compounds, **616**, (2014), 614-617.

[28] Z. Guo, et al., "ZnO/CuO hetero-hierarchical nanotrees array: hydrothermal preparation and self-cleaning properties." Langmuir **27**, (2011) 6193-6200

[29] H. Huang, et al., "Low-Temperature Growth of SnO2 Nanorod Arrays and Tunable n–p–n Sensing Response of a ZnO/SnO2 Heterojunction for Exclusive Hydrogen Sensors," Adv. Funct. Mater. **2011** (21), (2011) 2680–2686.

[30] S. T. Jun, G. M. Choi, "Composition Dependence of the Electrical Conductivity of ZnO(n)–CuO(p) Ceramic Composite," J. Am. Ceram. Soc. **81** (3), (2005) 695-699.

[31] A. Gurlo, N. Bârsan, A. Oprea, M. Sahm, T. Sahm and U. Weimar, An n- to p-type conductivity transition induced by oxygen adsorption on α-Fe_2O_3, Appl. Phys. Lett. **85**, (2004) 2280.